PHYSICAL REVIEW B **92**, 241409(R) (2015)

Tunneling in graphene–topological insulator hybrid devices

H. Steinberg,[1,2] L. A. Orona,[1] V. Fatemi,[1] J. D. Sanchez-Yamagishi,[1] K. Watanabe,[3] T. Taniguchi,[3] and P. Jarillo-Herrero[1,*]
[1]*Department of Physics, Massachusetts Institute of Technology, Cambridge, Massachusetts 02139, USA*
[2]*Racah Institute of Physics, The Hebrew University, Jerusalem 91904, Israel*
[3]*Advanced Materials Laboratory, National Institute of Material Science, 1-1 Namiki, Tsukuba 305-0044, Japan*
(Received 22 April 2015; revised manuscript received 10 November 2015; published 28 December 2015)

Hybrid graphene–topological insulator (TI) devices were fabricated using a mechanical transfer method and studied via electronic transport. Devices consisting of bilayer graphene (BLG) under the TI Bi_2Se_3 exhibit differential conductance characteristics which appear to be dominated by tunneling, roughly reproducing the Bi_2Se_3 density of states. Similar results were obtained for BLG on top of Bi_2Se_3, with tenfold greater conductance consistent with a larger contact area due to better surface conformity. The devices further show evidence of inelastic phonon-assisted tunneling processes involving both Bi_2Se_3 and graphene phonons. These processes favor phonons which compensate for momentum mismatch between the TI Γ and graphene K, K' points. Finally, the utility of these tunnel junctions is demonstrated on a density-tunable BLG device, where the charge neutrality point is traced along the energy-density trajectory. This trajectory is used as a measure of the ground-state density of states.

DOI: 10.1103/PhysRevB.92.241409 PACS number(s): 73.40.Gk, 73.50.−h, 73.20.At

The recently developed mechanical transfer technique [1], originally used for placing graphene on top of hexagonal boron nitride (h-BN), has emerged as a generic tool for creating a variety of vertical heterostructures of van der Waals (vdW) materials [2]. Of particular interest are those structures where current is driven across the material interface, such as tunnel devices realized using ultrathin h-BN layers as tunnel barriers either between graphene and an electrode [3] or between parallel graphene layers [4]. Devices realizing tunneling between parallel two-dimensional (2D) systems are useful as probes for a fundamental investigation of 2D materials [5] and are gaining traction as probes for graphene [6].

In this Rapid Communication we report on a type of tunnel device, realized at the interface of graphene and the topological insulator (TI) Bi_2Se_3. TIs host exotic 2D systems at their surface [7], and the potential to hybridize them with graphene is the subject of a recent theoretical effort [8–11]. These works generally assume that the graphene and TI bands couple strongly, leading to fundamental modifications to the graphene band structure, which is expected to inherit an enhanced spin-orbit (SO) coupling [8] and attain nontrivial spin textures [11].

The vdW structure of the TI Bi_2Se_3 allows for the fabrication of such hybrids using the mechanical transfer technique. We find that graphene and Bi_2Se_3 layers are weakly coupled, such that electronic transport between the graphene and TI layers is governed by tunneling. As tunneling into high quality graphene devices remains a considerable challenge, weakly coupled TIs may offer an alternative route to performing energy spectroscopy, probing the graphene density of states, inelastic properties, or for following the density dependence of spectral features. This is demonstrated on a density-tuned bilayer graphene (BLG) device, where deviations from a single-particle spectrum are observed. The latter, due to its flat density of states, can provide a useful probe for the TI density of states.

*pjarillo@mit.edu

Figure 1(a) shows device 1, "BLG bottom," where a Bi_2Se_3 flake is transferred on top of a BLG flake (outlined in green) deposited on SiO_2. The flakes are independently contacted by evaporated metallic electrodes [Fig. 1(b)]. The BLG-TI junctions are studied by measuring the differential conductance dI/dV versus applied bias voltage V_{SD} with the source on one material and the drain on the other (TI1 to G1). A four-probe geometry is realized by measuring the voltage across the opposing contacts [$V_{TI} = V(\text{TI2}) - V(\text{G2})$]. The dI/dV trace at $T = 4$ K of device 1 [Fig. 1(c)] shows a pronounced suppression at negative V_{TI} values, similar to scanning tunneling microscopy (STM) measurements taken on Bi_2Se_3 [12–14], where dI/dV is proportional to the density of states (DOS) and the suppression at negative bias is associated with the bulk gap of the Bi_2Se_3. The BLG-TI interface therefore behaves as an effective tunnel junction although no intentional barrier was placed between the materials. It is a remarkably robust junction, maintaining a stable signal while sustaining high voltage biases exceeding 0.5 V at negative bias.

The tunneling functionality of the graphene-Bi_2Se_3 interface could be a consequence of Bi_2Se_3 oxidation [15]. In over 20 devices studied, the interface resistance varied from 10 M$\Omega\,\mu$m^2 to 10 k$\Omega\,\mu$m^2, which could be associated with varying degrees of oxidation. The stability and high bias achieved by graphene-TI junctions, however, do not favor this explanation—oxide-based junctions rarely function at biases in excess of 200 meV [16]. Alternatively, the variation in interface resistance could arise due to differences in the effective contact area: Graphene conforms to the underlying substrate and has angstrom-scale height variations when deposited on SiO_2, resulting in an effective partial contact area. To test this we studied devices where BLG is deposited *on top* of Bi_2Se_3 ("BLG top"): In device 2 a single BLG flake covers two Bi_2Se_3 flakes [Figs. 1(d) and 1(e)]. Measured separately [red and blue curves in Fig. 1(f)], the two junctions exhibit comparable dI/dV characteristics which are very similar to the "graphene on bottom" devices (albeit with a smaller bias range).

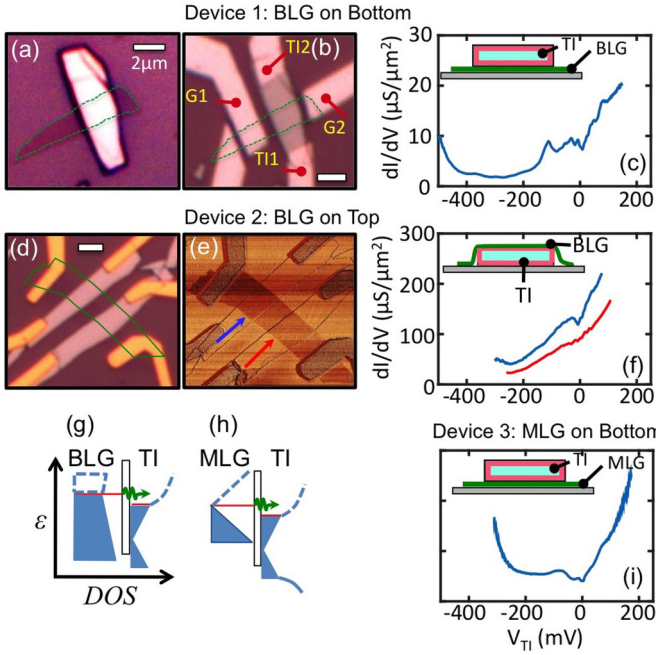

FIG. 1. (Color online) (a) Optical image of device 1, "BLG bottom," consisting of BLG on the bottom and Bi_2Se_3 on top. The BLG outline is marked in green. (b) Device 1 with contacts. The bar is 2 μm long. (c) dI/dV vs V_{TI} of device 1 (source on the Bi_2Se_3). Inset: Schematic showing the BLG (green) underneath the TI (teal, outline representing the TI surface states). (d) Device 2: "BLG top." A single BLG flake deposited on top of two Bi_2Se_3 flakes. (e) Atomic force microscopy phase image of device 2. The arrows mark the two separate junctions. (f) dI/dV vs V_{TI} of the two junctions in device 2. Top junction: blue; bottom: red. Inset: Schematic showing BLG on top of the TI. (g), (h) Annotations illustrating the DOS alignment in tunneling between (g) BLG and (h) monolayer graphene (MLG) and a TI. All dI/dV data are normalized per μm^2. (i) dI/dV vs V_{TI} of device 3: "MLG bottom."

The interface conductivity of "BLG top" junctions is an order of magnitude greater than "MLG/BLG on bottom" ones, indicating that the effective contact area is a plausible source of variation. It is not clear, however, what is the origin of the generic tunneling functionality. An interesting possibility is that the tunnel barrier is associated with the lack of direct chemical bonding between the two layers. Interlayer tunnel barriers in layered materials are observed in high T_c superconductors [17] and in vdW materials such as 4Hb-TaS_2 [18]. Incoherent interlayer transport was also reported in stacked twisted bilayer graphene devices [19], and graphene layers could be weakly coupled to the underlying graphite [20]. Testing this hypothesis would require further investigation.

As expected, the dI/dV characteristics vary with the choice of MLG vs BLG. The tunneling current is expressed as a convolution of the graphene DOS $\rho_G(\varepsilon)$ and the TI DOS $\rho_{TI}(\varepsilon)$ [21],

$$I \sim A \int_0^{eV} \rho_G(\varepsilon - eV)\rho_{TI}(\varepsilon)|t(\varepsilon)|^2 d\varepsilon, \qquad (1)$$

where A is the effective overlap area and $t(\varepsilon)$ stands for the tunnel coupling through the barrier. This expression is qualitatively depicted in the schematics in Figs. 1(g) and 1(h), showing ρ_G on the left and ρ_{TI} (including bulk and surface) on the right. For BLG devices [Fig. 1(g)], $\rho_G(\varepsilon)$ is relatively featureless away from charge neutrality, so the dI/dV curve is close to $\rho_{TI}(\varepsilon)$. This explains why BLG-TI dI/dV traces are similar to STM measurements of Bi_2Se_3. MLG-TI devices [Fig. 1(h)] have energy-dependent $\rho(\varepsilon)$ on both sides of the barrier, and device 3 [Fig. 1(i)] indeed exhibits a very different dI/dV characteristic, with a stronger suppression around zero bias which we associate with the graphene Dirac point (DP).

Tunnel junctions are useful in measuring inelastic spectra, where the onset of processes such as phonon-assisted tunneling appears as step-increase features in the differential conductance. These are detectable as peaks in the second derivative d^2I/dV^2 at bias voltages corresponding to the phonon energies. It is possible to differentiate between Bi_2Se_3 and graphene phonons because their respective spectra span different energy ranges (up to 20 meV for Bi_2Se_3 [23], and up to 200 meV for graphene [24]). Several devices exhibit well-developed inelastic spectra: Device 3, "MLG bottom" [Fig. 1(i)], has sharp, steplike features in dI/dV close to zero. The corresponding d^2I/dV^2 plot [Fig. 2(a)] shows peaks at ± 7.7 meV which coincide in device 3 (MLG) and in device 1 (BLG bottom). We associate this feature with a Bi_2Se_3 surface optical phonon previously identified using helium scattering at the same energy [25]. This phonon plays a role in suppressing surface transport [26], and inelastic tunneling data may be useful in probing its coupling to surface electrons.

Signatures of graphene phonons, appearing at higher bias voltages, are found in numerous devices. For example, device 4 [Fig. 2(b)] is a high quality "BLG bottom" device fabricated by deposition of BLG on h-BN followed by transferring Bi_2Se_3 on top. The d^2I/dV^2 plot shows a prominent peak at 67 meV, corresponding to the energy of the graphene out-of-plane acoustic/optical (ZA/ZO) mode at the K, K' points. This phonon is seen in many graphene and graphite tunneling experiments both in devices [3] and in STM [27,28], and is generally believed to assist the tunneling process by

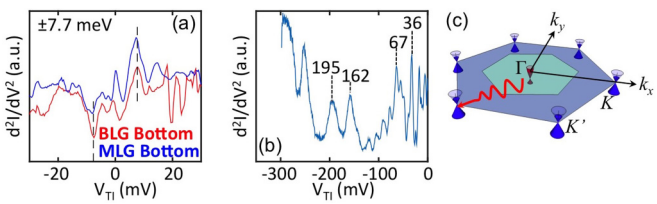

FIG. 2. (Color online) (a) d^2I/dV^2 vs V_{TI} of device 1 (BLG bottom) and device 3 (MLG bottom). Both devices exhibit a peak in the second derivative, corresponding to an inelastic excitation, at 7.7 meV, associated with a Bi_2Se_3 optical phonon. (b) $|d^2I/dV^2|$ vs V_{TI} of device 4, "BLG bottom," exhibiting a rich spectrum of inelastic features. The energies marked in the figure are discussed in the text. (c) Phonon-assisted tunneling in momentum mismatched materials: Tunneling from the TI states at the Γ point to graphene states at the K, K' points is assisted by Brillouin zone (BZ)-edge phonons (wavy red line). The TI first Brillouin zone is drawn in teal. It is assumed to have an arbitrary angle to the graphene orientation.

providing the momentum required to inject an electron to the K, K' points. In our devices, where graphene and Bi_2Se_3 Fermi surface momenta are highly mismatched, it is likely that the same phonon is required to allow momentum-conserving tunneling from low energy Bi_2Se_3 states, centered at the Γ point, to the graphene K, K' points [schematic in Fig. 2(c)]. Device 4 also exhibits a feature at 162 meV associated with the longitudinal acoustic (LA)/longitudinal optic (LO) mode, also a K, K' phonon, and a feature at 195 meV associated with the transverse optical (TO) mode at Γ. Other features (e.g., a phonon at 36 meV) could be associated with the h-BN substrate [3].

In the rest of this Rapid Communication we focus on "BLG bottom" device 5. Device 5 can be measured by BLG in-plane transport (G1–G2) or by tunneling (T1–G1). In-plane resistance $R_{2T}(V_{TI}, V_{BG})$ is presented in Fig. 3(c), showing a resistance peak when the chemical potential crosses the BLG charge neutrality point (CNP). The Bi_2Se_3 electrode acts as a well-behaved gate, and the small tunneling current does not interfere with the in-plane measurement. The resistance map is typical of doubly gated graphene [29,30], where the diagonal feature corresponds to a high resistance state in the BLG region underneath the TI. This feature intercepts $V_{TI} = 0$ at $V_{BG} = V_0 = 20$ V, indicating that the BLG is p doped and the CNP is energetically mismatched from the TI DP [Fig. 3(a), annotation I]. Its slope is dictated by the requirement that the top and bottom gates compensate each other's charge (annotation II) and therefore follows the ratio C_{BG}/C_{TI} (C_{TI} and C_{BG} are the graphene-TI and graphene–back-gate capacitances, respectively). Using this relation, we extract the geometric capacitance of the TI-BLG junction $C_{TI} = 1.3 \times 10^{-2}$ F/m^2, 110 times greater than the back-gate capacitance. Both the relative permittivity of the interlayer medium ε and the graphene-Bi_2Se_3 effective distance d are unknown. However, the measured value of C_{TI} fixes their ratio to 1.5 nm^{-1}. As the interface is a tunnel junction, d is unlikely to exceed 3 nm, setting a limit of $\varepsilon < 5$.

Gate-dependent tunneling measurements are presented in Figs. 3(d) and 3(e): Such measurements are sensitive to energy shifts in the spectral features due to the changes in density. In Fig. 3(d) it is clear that the underlying structure of the Bi_2Se_3 gap at negative V_{TI} is retained while a set of features closer to zero bias evolve with V_{BG}. To trace these features we plot the second derivative d^2I/dV^2 as a color map in Fig. 3(e). The data exhibit a set of diagonal features with opposite slopes and gate-independent features which appear as faint vertical lines. The latter gate-independent features are enhanced by averaging over all back-gate values [Fig. 3(b)], where we again find the ZA/ZO phonon features at ± 65 meV. The 22 meV feature coincides with the energy of the Bi_2Se_3 A_{1g}^2 phonon [23].

V_{BG} changes the graphene density, vertically shifting the band structure [Fig. 3(a), annotation III]. To trace a spectral feature such as the CNP, a voltage δV_{TI} has to be applied to compensate for the density-induced change in chemical potential, $\delta\mu_G$. This is formulated as

$$e\delta V_{TI} = \delta\mu_G. \tag{2}$$

To trace the spectral features on the $V_{TI} - V_{BG}$ plane, we have to note that planar tunneling electrodes are large capacitors which charge the graphene layer at finite bias, as discussed earlier. The equations governing the charging of the

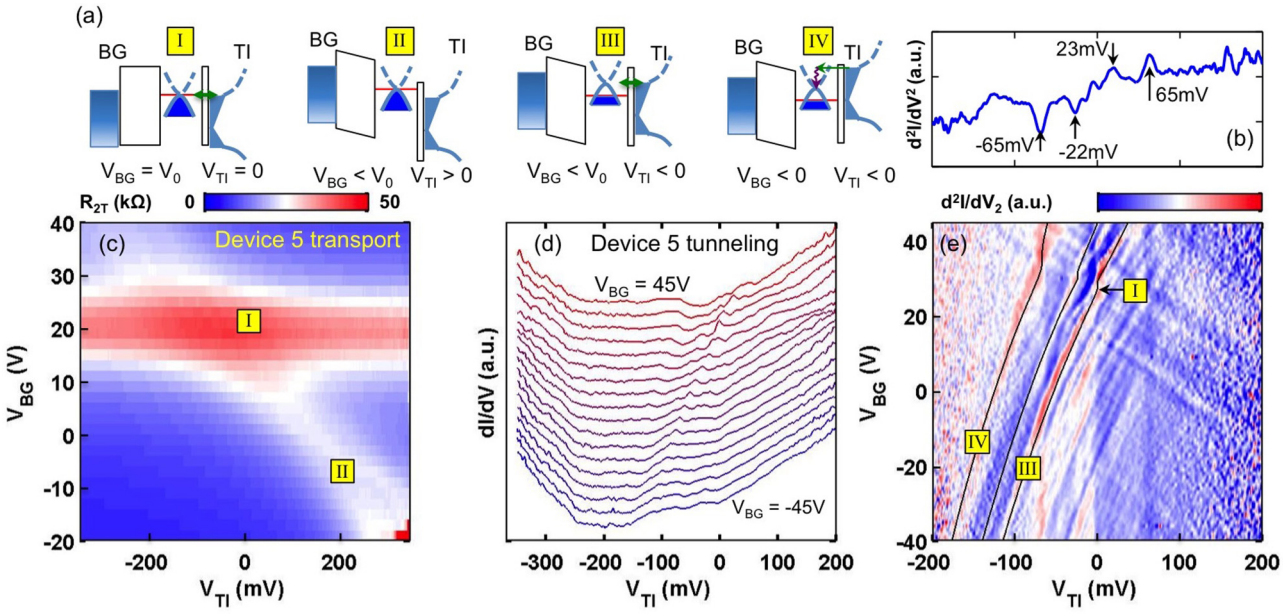

FIG. 3. (Color online) (a) Schematics of gate-dependent tunneling and transport processes. (I) BLG at $n = 0$, V_{TI} at zero bias. (II) Tracing the CNP in a transport measurement: V_{BG} and V_{TG} are balanced to keep $n = 0$. (III) Tunneling into the CNP: $V_{BG} < 0$ tunes the BLG to $n > 0$, $V_{TI} < 0$ keeps tunneling to the CNP. (IV) Phonon-assisted tunneling into the CNP. (b) d^2I/dV^2 vs V_{TI} obtained from integrating data in (e). (c) In-plane electronic transport vs V_{BG} and V_{TI}. Annotation II marks the CNP diagonal trajectory. Annotation I marks the point where this trajectory crosses $V_{TI} = 0$. (d) dI/dV vs V_{TI} at a range of gate voltage (5 V interval). (e) d^2I/dV^2 vs V_{TI} and V_{BG}. Annotations mark the elastic process (III) and phonon-assisted processes (IV). The lines superimposed on the data are fits to the trajectories of elastic and inelastic tunneling into the CNP [22].

graphene layer connect the incremental gate voltages $\delta V_{\mathrm{TI,BG}}$ to the incremental charges on the back gate and TI $\delta n_{\mathrm{BG,TI}}$,

$$-e\delta n_i = C_i\left(\delta V_i - \frac{\delta\mu_{\mathrm{G}}}{e}\right), \tag{3}$$

where $i = \mathrm{BG,TI}$.

Interestingly the CNP tunneling condition in Eq. (2) also ensures that there will be no extra charge accumulated on the TI ($\delta n_{\mathrm{TI}} = 0$), as the argument in parentheses in Eq. (3) remains zero. More generally, this means that constant energy features lie on trajectories which keep the charge on the tunneling electrode fixed. In the Supplemental Material (SM) [22] we derive the CNP-tunneling trajectory and find its slope to be

$$\frac{\delta V_{\mathrm{TI}}}{\delta V_{\mathrm{BG}}} = \frac{C_{\mathrm{BG}}}{C_Q + C_{\mathrm{BG}}}, \tag{4}$$

where $C_Q = e^2\rho$ is the quantum capacitance of the BLG. The slope is independent of C_{TI}, consistent with the induced charge on the TI remaining zero.

As a result, Eq. (4) can be used to evaluate C_Q by fitting the slope of the features appearing in the figure. The most prominent feature in Fig. 3(e), marked by "III," is likely the charge neutrality point, which attains a cusp in the DOS due to a finite displacement field (annotation I). The slope of this feature is not constant, and appears to vary along the trajectory (Fig. S1 [22]). This indicates that C_Q, and hence the DOS, changes with density, as expected for the hyperbolic dispersion of BLG [31–33].

We fit the expected trajectory [Fig. 3(e), feature "III"]. To calculate this fit it is crucial to acknowledge that the BLG dispersion varies within the V_{BG}-V_{TI} plane, where at each point the displacement field is different. The calculation, described in the SM [22], is carried out self-consistently, using an approximate trajectory for calculating the displacement field at each value of V_{BG} and V_{TI}. We then extract $n(\varepsilon)$, $\rho(n)$, and finally C_Q, and integrate the trajectory from the slope in Eq. (4). The calculation is refined iteratively. Using the Fermi velocity v_F as a fitting parameter, the full trajectory can be reproduced with $v_F = 1.06 \times 10^6$ m/s, in good agreement with noninteracting values for BLG.

Multiple replicas [marked by IV in Fig. 3(e)] of the CNP tunneling feature appear as lines running parallel to the elastic feature ("IV"). They are associated with phonon-assisted inelastic tunneling processes to the CNP. Unlike the gate-independent phonon-onset features discussed above, where tunneling takes place to the Fermi energy, these features represent phonon-assisted tunneling to some sharp spectral feature (here the CNP), and evolve with the gate in parallel to the elastic tunneling feature. Their trajectories, presented in Fig. S1 [22], should depend on the elastic feature, after accounting for modified displacement fields at higher bias. However, to fit the actual data we find that the Fermi velocities have to be modified in each of the inelastic features (assuming interlayer coupling $t_\perp$ remains fixed). The modified Fermi velocities are 0.98×10^6 m/s for the -22 mV feature, and 0.9×10^6 m/s for the -65 mV feature. This points, perhaps, to velocity renormalization.

In summary, the graphene-Bi_2Se_3 interface is a high quality tunnel junction which can be integrated in to a density-tunable device. Further studies are required to address the effect of junction properties, such as crystallographic orientation, interface quality, and the effect of Bi_2Se_3 oxidation. Phonon-assisted tunneling is observed at finite bias, with specific phonon-activation processes which bridge the mismatch in crystal momentum between the two materials. Nevertheless, tunneling in general is not momentum conserving, probably due to junction inhomogeneity or other scattering processes. The role of the surface state in the tunneling process is also an open question: Where some devices (device 1) seem to reveal evidence of bulk states in the tunneling signal, others (device 4) appear to be mostly surface dominated.

This work was supported by the DOE Basic Energy Science Office, Division of Materials Sciences and Engineering, under Award No. DE-SC0006418. This work made use of the Materials Research Science and Engineering Center Shared Experimental Facilities supported by NSF under Grant No. DMR-0819762. Sample fabrication was performed partly at the Harvard Center for Nanoscale Science supported by the NSF under Grant No. ECS-0335765. H.S. acknowledges support from Marie Curie CIG Grant No. PCIG12-GA-2012-333620.

[1] C. R. Dean, A. F. Young, I. Meric, C. Lee, L. Wang, S. Sorgenfrei, K. Watanabe, T. Taniguchi, P. Kim, K. L. Shepard, and J. Hone, Nat. Nanotechnol. **5**, 722 (2010).

[2] A. K. Geim and I. Grigorieva, Nature (London) **499**, 419 (2013).

[3] F. Amet, J. R. Williams, A. G. F. Garcia, M. Yankowitz, K. Watanabe, T. Taniguchi, and D. Goldhaber-Gordon, Phys. Rev. B **85**, 073405 (2012).

[4] T. Georgiou, R. Jalil, B. D. Belle, L. Britnell, R. V. Gorbachev, S. V. Morozov, Y.-J. Kim, A. Gholinia, S. J. Haigh, O. Makarovsky, L. Eaves, L. A. Ponomarenko, A. K. Geim, K. S. Novoselov, and A. Mishchenko, Nat. Nanotechnol. **8**, 100 (2013).

[5] J. P. Eisenstein, T. J. Gramila, L. N. Pfeiffer, and K. W. West, Phys. Rev. B **44**, 6511 (1991).

[6] L. Britnell, R. V. Gorbachev, A. K. Geim, L. A. Ponomarenko, A. Mishchenko, M. T. Greenway, T. M. Fromhold, K. S. Novoselov, and L. Eaves, Nat. Commun. **4**, 1794 (2013).

[7] M. Z. Hasan and C. L. Kane, Rev. Mod. Phys. **82**, 3045 (2010).

[8] K.-H. Jin and S.-H. Jhi, Phys. Rev. B **87**, 075442 (2013).

[9] W. Liu, X. Peng, X. Wei, H. Yang, G. M. Stocks, and J. Zhong, Phys. Rev. B **87**, 205315 (2013).

[10] L. Kou, B. Yan, F. Hu, S.-C. Wu, T. O. Wehling, C. Felser, C. Chen, and T. Frauenheim, Nano Lett. **13**, 6251 (2013).

[11] J. Zhang, C. Triola, and E. Rossi, Phys. Rev. Lett. **112**, 096802 (2014).

[12] Z. Alpichshev, R. R. Biswas, A. V. Balatsky, J. G. Analytis, J.-H. Chu, I. R. Fisher, and A. Kapitulnik, Phys. Rev. Lett. **108**, 206402 (2012).

[13] P. Cheng, C. Song, T. Zhang, Y. Zhang, Y. Wang, J.-F. Jia, J. Wang, Y. Wang, B.-F. Zhu, X. Chen, X. Ma, K. He, L. Wang, X. Dai, Z. Fang, X. Xie, X.-L. Qi, C.-X. Liu, S.-C. Zhang, and Q.-K. Xue, Phys. Rev. Lett. **105**, 076801 (2010).

[14] T. Hanaguri, K. Igarashi, M. Kawamura, H. Takagi, and T. Sasagawa, Phys. Rev. B **82**, 081305(R) (2010).

[15] D. Kong, J. J. Cha, K. Lai, H. Peng, J. G. Analytis, S. Meister, Y. Chen, H.-J. Zhang, I. R. Fisher, Z.-X. Shen, and Y. Cui, ACS Nano **5**, 4698 (2011).

[16] D. C. Tsui, Phys. Rev. Lett. **24**, 303 (1970).

[17] R. Kleiner and P. Müller, Phys. Rev. B **49**, 1327 (1994).

[18] W. Wattamaniuk, J. Tidman, and R. Frindt, Phys. Rev. Lett. **35**, 62 (1975).

[19] Y. Kim, H. Yun, S.-G. Nam, M. Son, D. S. Lee, D. C. Kim, S. Seo, H. C. Choi, H.-J. Lee, S. W. Lee, and J. S. Kim, Phys. Rev. Lett. **110**, 096602 (2013).

[20] G. Li and E. Y. Andrei, Nat. Phys. **3**, 623 (2007).

[21] E. L. Wolf, *Principles of Electron Tunneling Spectroscopy*, International Series on Monographs on Physics (Oxford University Press, New York, 2012).

[22] See Supplemental Material at http://link.aps.org/supplemental/10.1103/PhysRevB.92.241409 for a detailed derivation of the charging model and comparison of transport and tunneling data.

[23] X. Zhu, L. Santos, R. Sankar, S. Chikara, C. Howard, F. C. Chou, C. Chamon, and M. El-Batanouny, Phys. Rev. Lett. **107**, 186102 (2011).

[24] L. Wirtz and A. Rubio, Solid State Commun. **131**, 141 (2004).

[25] X. Zhu, L. Santos, C. Howard, R. Sankar, F. C. Chou, C. Chamon, and M. El-Batanouny, Phys. Rev. Lett. **108**, 185501 (2012).

[26] M. V. Costache, I. Neumann, J. F. Sierra, V. Marinova, M. M. Gospodinov, S. Roche, and S. O. Valenzuela, Phys. Rev. Lett. **112**, 086601 (2014).

[27] Y. Zhang, V. W. Brar, F. Wang, Ç. Girit, Y. Yayon, M. Panlasigui, A. Zettl, and M. F. Crommie, Nat. Phys. **4**, 627 (2008).

[28] V. W. Brar, S. Wickenburg, M. Panlasigui, C.-H. Park, T. O. Wehling, Y. Zhang, R. Decker, Ç. Girit, A. V. Balatsky, S. G. Louie, A. Zettl, and M. F. Crommie, Phys. Rev. Lett. **104**, 036805 (2010).

[29] B. Huard, J. A. Sulpizio, N. Stander, K. Todd, B. Yang, and D. Goldhaber-Gordon, Phys. Rev. Lett. **98**, 236803 (2007).

[30] T. Taychatanapat and P. Jarillo-Herrero, Phys. Rev. Lett. **105**, 166601 (2010).

[31] S. Das Sarma, S. Adam, E. H. Hwang, and E. Rossi, Rev. Mod. Phys. **83**, 407 (2011).

[32] A. H. Castro Neto, F. Guinea, N. M. R. Peres, K. S. Novoselov, and A. K. Geim, Rev. Mod. Phys. **81**, 109 (2009).

[33] E. McCann, Phys. Rev. B **74**, 161403 (2006).